Broadband optical absorptions in inversed woodpile metallic photonic crystals

Md M. Hossain and Min Gu*

Centre for Micro-Photonics and CUDOS, Faculty of Engineering and Industrial Sciences, Swinbnurne University of Technology, Hawthorn, Victoria 3122, Australia
**mgu@swin.edu.au*

Abstract: Here we demonstrate enhanced optical absorptions within three-dimensional inversed woodpile metallic photonic crystals fabricated via the combination of the direct laser writing method and the electrodeposition method. These metallic microstructures operating in the optical wavelengths are found to possess multiple enhanced absorption peaks over a broad spectral range. We characterize the optical properties with detailed numerical simulations and show that the broadband enhanced absorptions originate from the excitation of robust localized plasmon resonances and enhanced interactions at the photonic band edge within the metallic photonic crystals.

OCIS codes: (230.5298) Photonic crystals; (160.4760) Optical properties; (250.5403) Plasmonics.

References and links

1. T. V. Teperik, V. V. Popov, and F. J. Garcia De Abajo, "Void plasmons and total absorption of light in nanoporous metallic films," Phys. Rev. B **71**(8), 085408 (2005).
2. Y. Q. Ye, Y. Jin, and S. He, "Omnidirectional, polarization-insensitive and broadband thin absorber in the terahertz regime," J. Opt. Soc. Am. B **27**(3), 498–504 (2010).
3. S. Collin, F. Pardo, R. Teissier, and J. L. Pelouard, "Efficient light absorption in metal-semiconductor-metal nanostructures," Appl. Phys. Lett. **85**(2), 194–196 (2004).
4. E. Popov, D. Maystre, R. C. McPhedran, M. Nevière, M. C. Hutley, and G. H. Derrick, "Total absorption of unpolarized light by crossed gratings," Opt. Express **16**(9), 6146–6155 (2008).
5. N. Bonod, G. Tayeb, D. Maystre, S. Enoch, and E. Popov, "Total absorption of light by lamellar metallic gratings," Opt. Express **16**(20), 15431–15438 (2008).
6. T. V. Teperik, F. J. García De Abajo, A. G. Borisov, M. Abdelsalam, P. N. Bartlett, Y. Sugawara, and J. J. Baumberg, "Omnidirectional absorption in nanostructured metal surfaces," Nat. Photonics **2**(5), 299–301 (2008).
7. J. G. Fleming, S. Y. Lin, I. El-Kady, R. Biswas, and K. M. Ho, "All-metallic three-dimensional photonic crystals with a large infrared bandgap," Nature **417**(6884), 52–55 (2002).
8. S. Y. Lin, J. G. Fleming, and I. El-Kady, "Three-dimensional photonic-crystal emission through thermal excitation," Opt. Lett. **28**(20), 1909–1911 (2003).
9. S. Y. Lin, J. G. Fleming, Z. Y. Li, I. El-Kady, R. Biswas, and K. M. Ho, "Origin of absorption enhancement in a tungsten, three-dimensional photonic crystal," J. Opt. Soc. Am. B **20**(7), 1538–1541 (2003).
10. M. M. Hossain, G. Chen, B. Jia, X. H. Wang, and M. Gu, "Optimization of enhanced absorption in 3D-woodpile metallic photonic crystals," Opt. Express **18**(9), 9048–9054 (2010).
11. J. Li, M. M. Hossain, B. Jia, D. Buso, and M. Gu, "Three-dimensional hybrid photonic crystals merged with localized plasmon resonances," Opt. Express **18**(5), 4491–4498 (2010).
12. H. Y. Sang, Z. Y. Li, and B. Y. Gu, "Engineering the structure-induced enhanced absorption in three-dimensional metallic photonic crystals," Phys. Rev. E Stat. Nonlin. Soft Matter Phys. **70**(6), 066611 (2004).
13. S. Y. Lin, J. Moreno, and J. G. Fleming, "Three-dimensional photonic-crystal emitter for thermal photovoltaic power generation," Appl. Phys. Lett. **83**(2), 380–382 (2003).
14. S. E. Han, A. Stein, and D. J. Norris, "Tailoring self-assembled metallic photonic crystals for modified thermal emission," Phys. Rev. Lett. **99**(5), 053906 (2007).
15. P. Nagpal, S. E. Han, A. Stein, and D. J. Norris, "Efficient low-temperature thermophotovoltaic emitters from metallic photonic crystals," Nano Lett. **8**(10), 3238–3243 (2008).
16. H. A. Atwater and A. Polman, "Plasmonics for improved photovoltaic devices," Nat. Mater. **9**(3), 205–213 (2010).
17. F. Hallermann, C. Rockstuhl, S. Fahr, G. Seifert, S. Wackerow, H. Graener, G. V. Plessen, and F. Lederer, "On the use of localized plasmon polaritons in solar cells," Phys. Status Solidi A **205**(12), 2844–2861 (2008).

#169293 - $15.00 USD Received 24 May 2012; revised 28 Jun 2012; accepted 28 Jun 2012; published 2 Jul 2012

18. V. E. Ferry, L. A. Sweatlock, D. Pacifici, and H. A. Atwater, "Plasmonic nanostructure design for efficient light coupling into solar cells," Nano Lett. **8**(12), 4391–4397 (2008).
19. J. H. Lee, Y. S. Kim, K. Constant, and K. M. Ho, "Woodpile metallic photonic crystals fabricated by using soft lithography for tailored thermal emission," Adv. Mater. (Deerfield Beach Fla.) **19**(6), 791–794 (2007).
20. E. Nicoletti, D. Bulla, B. Luther-Davies, and M. Gu, "Planar defects in three-dimensional chalcogenide glass photonic crystals," Opt. Lett. **36**(12), 2248–2250 (2011).
21. I. Staude, M. Thiel, S. Essig, C. Wolff, K. Busch, G. von Freymann, and M. Wegener, "Fabrication and characterization of silicon woodpile photonic crystals with a complete bandgap at telecom wavelengths," Opt. Lett. **35**(7), 1094–1096 (2010).
22. E. D. Palik, *Handbook of Optical Constants of Solids* (Academic Press, San Diego, 1998).

1. Introduction

Efficient optical absorbers are of key interest for numerous photonics applications. Metals, in general, are weakly dissipative in the optical wavelengths regime with their intrinsic dispersive features. However, metallic photonic microstructures with special geometries can lead to unique electromagnetic (EM) features compared to the bulk metal properties. Resonant light absorptions triggered by plasmon resonances have been reported in planar and in three-dimensional (3D) plasmonic nanostrucutres [1–3]. Total light absorption assisted with surface plasmons (SPs) has been reported in lamellar and crossed metallic gratings [4,5]. Moreover, omnidirectional absorption of light has been demonstrated in nanoporous metallic surfaces with the excitation of localized void plasmon resonances [6]. Plasmonic nanostructures with enhanced optical absorptions have potential applications in plasmonic solar cells. However, enhanced optical absorptions over a broad spectra is still challenging to achieve, which is crucial for potential applications. On the other hand, enhanced absorption has also been reported in periodic metallic microstructures, i.e. metallic photonic crystals (MPCs) [7–11]. This enhanced absorption takes place at the photonic band edge (in the vicinity of the transmission band) of the MPC structures [9,10,12]. These MPCs with enhanced absorption and wide photonic band gaps are capable of modified thermal emission and have potential applications in thermo-photovoltaics [13–15]. However, the functionality of MPCs relies on the cost-effective fabrication method realizing high quality MPC structures operating in the optical wavelengths which is challenging to achieve.

In this report, we demonstrate enhanced optical absorptions in a new kind of inversed woodpile MPCs operating in the optical wavelengths. The optical properties of the fabricated MPCs are unique in the sense that they possess broadband enhanced absorptions triggered by two different physical mechanisms. Firstly, the formations of cavity-like localized plasmon resonances within the 3D inversed woodpile MPC structures lead to strong field enhancement confined within the cavities and thus produce resonant optical absorptions. Secondly, enhanced absorption results within the MPC structures due to the strong EM interactions at the photonic band edge within the MPC environment. Indeed, the combination of the state-of-the-art direct laser writing (DLW) method for dielectric photonic crystal (PC) fabrication and electrodeposition method for metal infiltration provides an ideal platform to introduce multiple enhanced absorption peaks within the novel inversed woodpile MPCs. The ability of delivering enhanced absorptions with both plasmon resonances and band edge effects within the 3D MPCs offer the potential applications in plasmonic solar cells with the strong local field enhancment [16–18] and in desiging efficient thermal emitters [8,13,15].

#169293 - $15.00 USD Received 24 May 2012; revised 28 Jun 2012; accepted 28 Jun 2012; published 2 Jul 2012

2. Inversed woodpile MPCs

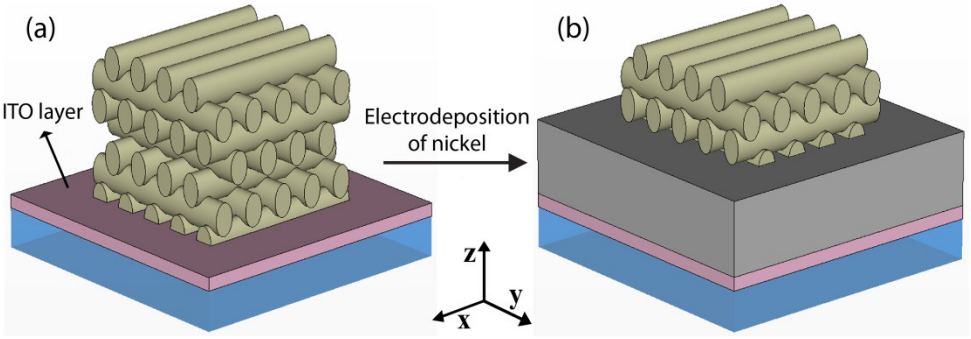

Fig. 1. Schematic diagram of the fabrication of inversed woodpile MPCs (a) Woodpile dielectric PC template on the ITO coated cover slip. (b) Metal is infiltrated into the woodpile PC template.

We employed the state-of-the-art direct laser writing (DLW) nanofabrication method to realize 3D dielectric woodpile photonic crystal (PC) microstructure templates. The DLW fabrication was performed on indium-tin-oxide coated glass substrates. For the realization of the MPCs nickel was infiltrated into the 3D dielectric PC microstructure templates by the electrodeposition method which eventually results in inversed woodpile nickel MPCs. The optical properties of nickel is promising for the realization of the potential applications of MPCs as it is highly reflective in the mid-infrared and fairly reflective in the near-infrared (NIR) wavelength (>1.0 μm) regions. Moreover, compared to other metals (which can be electrodeposited) such as gold, nickel is inexpensive, which makes nickel an ideal candidate to realize MPCs for practical applications. Electrodeposition has also been used to infiltrate nickel into the woodpile PCs fabricated by soft lithography [19]. However, it should be noted that the operating wavelengths of those fabricated metallic microstructure lies within 2-10 μm which is longer than the wavelength region of our interest. Moreover, the DLW fabrication method has allowed us to produce plasmon resonances with our inversed woodpile MPCs. The schematic of the fabrication procedure for achieving inversed woodpile MPCs is illustrated in Fig. 1.

The DLW fabrication of dielectric PCs was performed on thin layer of ITO coated glass coverslips (70-100Ω, SPI Supplies). For the DLW fabrication, a beam of femtosecond (~150 fs) laser pulses at a repetition rate of 76 MHz and at a wavelength of 580 nm was focused into the commercial liquid photoresist IP-L (Nanoscribe Gmbh) with an oil-immersion high NA objective (Olympus, NA = 1.4, 100 ×). The 3D woodpile geometries were written by the 3D translation of the liquid photoresist mounted on a piezoelectric scanning stage (P562, Physik Instrumente). A layer-by-layer fabrication approach was adopted for providing the mechanical stability of the woodpile PC template microstructures. To achieve an inversed MPC structure with an appropriate filling ratio, the multiline laser scanning method for the DLW microfabrication was employed [20,21]. In combination with the appropriate fabrication power and multiline laser scanning with a fixed displacement, polymerized lines of width 700 nm with a lowest aspect ratio of ~1.24 was realized. The in-plane lattice parameter for the polymer PC template was kept as 1.5 μm for a constant interlayer spacing of 0.6 μm. The lateral dimension of the PC template was 60 μm × 60 μm with a total sample thickness of seven layers.

#169293 - $15.00 USD Received 24 May 2012; revised 28 Jun 2012; accepted 28 Jun 2012; published 2 Jul 2012

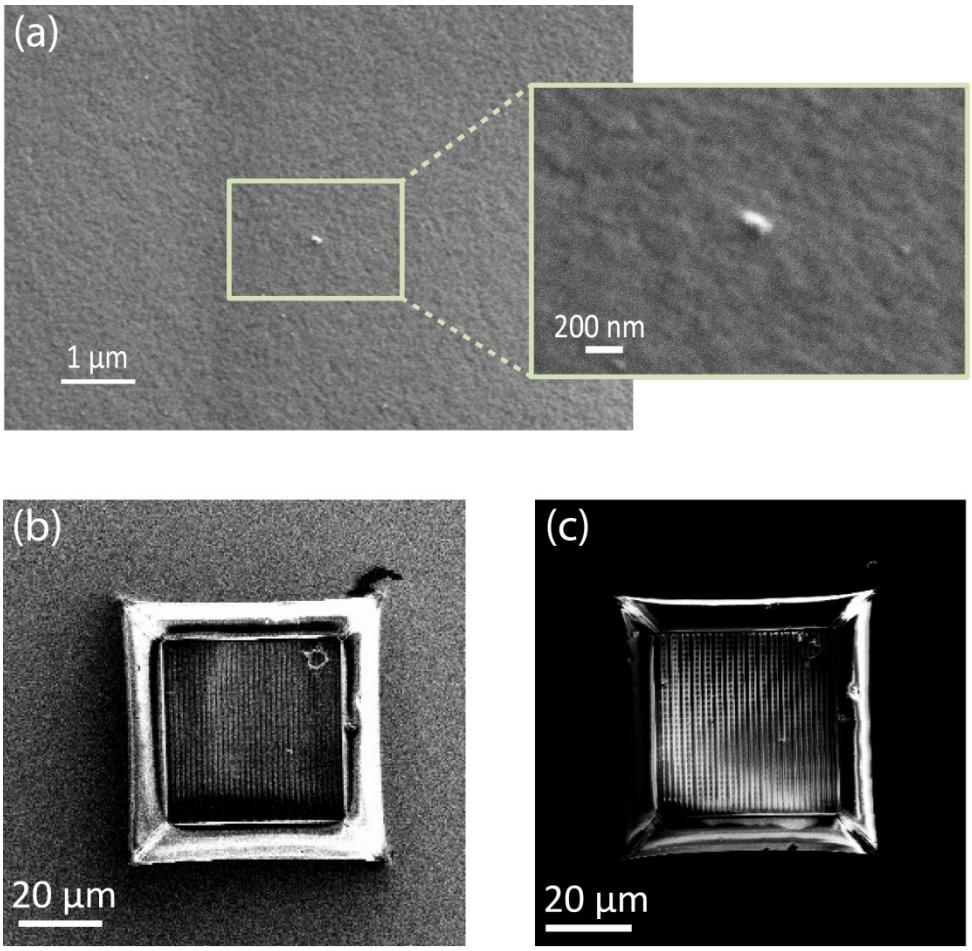

Fig. 2. (a) SEM images of an electrodeposited nickel film on an ITO coated glass substrate. Inset shows the magnified view of the high quality nickel film with a dust particle in the middle. (b) SEM image of a nickel infiltrated woodpile PC. (c) High contrast image showing the top layers of the woodpile microstructure.

For the electrodeposition of nickel, the conductive ITO layer of the glass coverslip worked as a cathode. ITO layered glasses are also highly transparent in the optical wavelengths region. The transparency drops in the longer wavelengths with higher conductivity of the ITO coating. Our ITO coated glass coverslips have high transmission of around 70-80% in the 1.0 µm to 3.0 µm wavelengths region which perfectly fits our experimental requirements. Before the DLW fabrication, the ITO glass coverslips were cleaned with ethanol and then thoroughly rinsed with distilled water. The glass coverslips were then heated to 75°C into a commercially available water-based detergent (Caswell) for 5 minutes for further cleaning and followed by rinsing with distilled water. After the DLW fabrication the ITO glass coverslips were again thoroughly rinsed with distilled water. For the electrodeposition of nickel, we used commercially available (Bright Nickel Plating Kit, Caswell) electrodeposition kit. An aqueous electrolyte solution of 20% weight in concentration of nickel salts was prepared for the electrodeposition. The pH value was for 4.0. An air pressure recycling procedure was followed for the PC microstructure templates for making the template surfaces wet by the electrolyte solution as employed in the previous works [19]. The electrodeposition was performed with an average current density of 1.23 mA/cm^2 with continuous stirring of the electrolyte solution. A homogeneous nickel film of thickness of 1.8 µm was achieved after the

#169293 - $15.00 USD Received 24 May 2012; revised 28 Jun 2012; accepted 28 Jun 2012; published 2 Jul 2012

electrodeposition. The thickness of the nickel film was intentionally kept as almost half to the PC structure thickness so that it did not overfill the PC template as can be understood from Fig. 1(b). After the electrodeposition the polymer PC template was left unremoved.

Figure 2(a) depicts the scanning electron microscope (SEM) images (top view) of the high quality electrodeposited nickel films onto the ITO coated substrate. Figure 2(b) shows the SEM image of the nickel infiltrated woodpile polymer PC i.e. inversed woodpile nickel MPC. It should be noted that the image was not very clear because of the charging effects i.e. the bright illumination forming in the top surface of the sample shown in Fig. 2(b) in SEM imaging. This was due to the fact that the top portion of the PC template was not filled with metal as can be understood from Fig. 1(b) and hence lacks electrical conductivity to achieve a better SEM image. To obtain a clear view, the same image shown in Fig. 2(b) was taken again with greatly reducing the brightness and enhancing the contrast of the sample under the SEM. The polymer rods at the top layer can be clearly viewed in Fig. 2(c) due to their greater thickness as obtained by the multiline laser scanning fabrication of the woodpile PC template.

Experimental characterization of the transmission and the reflection spectra were performed by using a Nicolet Nexus Fourier-transform infrared (FTIR) spectrometer with a continuum infrared microscope (Thermo Nicolet, Madison, Wisconsin, USA). The reflective 32x NA 0.65 objective (Reflechromat, Thermo Nicolet) provided a hollow light cone with an angle range of 18° to 41°. The experimental reflection spectrum of the MPC sample measured with an unpolarized incident light beam is shown in Fig. 3(a). The measurement shows a maximum of 80% reflection with multiple reflection dips starting from long wavelengths of 2.4 µm, 1.97 µm and 1.68 µm and so on to the shorter wavelengths. A transmission measurement was also carried out for the sample; however, almost no transmission was detected. This clearly suggests that the strong dips in the measured broad reflection spectrum i.e. within the wide band gap of the MPC are caused by the enhanced absorptions within the inversed woodpile MPC.

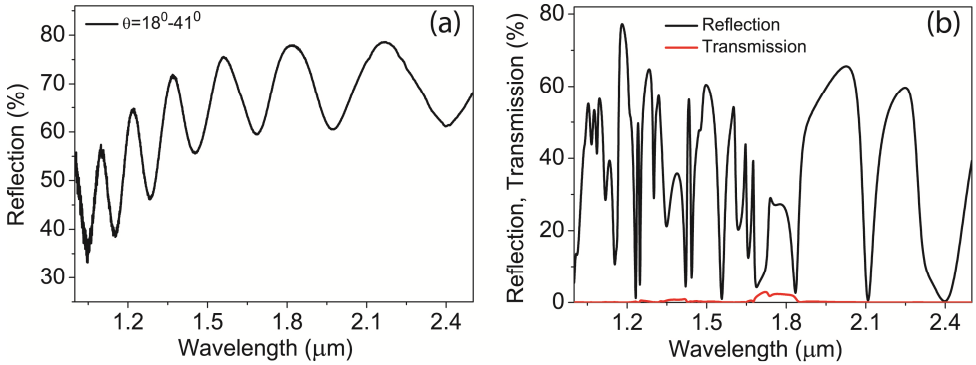

Fig. 3. (a) FTIR reflection measurement of the inversed woodpile nickel MPC sample with the angle of incidence of 18°-41°. (b) Calculated reflection and transmission spectra of the inversed woodpile nickel MPC with an angle of incidence of 25°.

3. Numerical characterization

To compare the experimental results, we performed numerical calculations based on the finite element method in frequency domain using the commercially available software (CST MWS). The dispersive properties of the bulk nickel were adopted from the handbook of optical constants of solids [22]. A refractive index of 1.52 was used for the polymer material. A linearly polarized plane wave with an angle of incidence of 25° (to account for the average angle of incidence in the experimental measurement) was used as the source of excitation for the transmission/reflection calculation and periodic boundary conditions were applied in the lateral directions. For simulations, the geometry of the MPC structure was considered same as in Fig. 2(b) where the nickel film thickness was half the thickness of the MPC sample. Figure

#169293 - $15.00 USD Received 24 May 2012; revised 28 Jun 2012; accepted 28 Jun 2012; published 2 Jul 2012

3(b) shows the calculated reflection and transmission spectra of the MPC structure. It can be noticed that the transmission over the entire spectral domain was minimal; only a maximum of 2.9% transmission was observed at the wavelength of 1.72 µm. Due to this small magnitude, the transmission was not detected within the experimental measurements. Furthermore, the reflection spectra contain multiple sharp dips caused by the enhanced absorptions in MPCs. However, the calculated reflection dips are much higher in strength compared to the experimentally measured ones as can be found in Fig. 3(a). The reason behind is that the reflection dips became broadened in the spectral width and weakened in magnitude due to the averaging effects caused in the experimental measurements with a finite wide opening angle. The spectral positions of the first three calculated reflection dips in the longer wavelengths presented in Fig. 3(b) are fairly comparable to that of the measured ones shown in Fig. 3(a). Some discrepancies can result from the structural imperfections and also from the broad angle of incidence FTIR spectroscopy measurement.

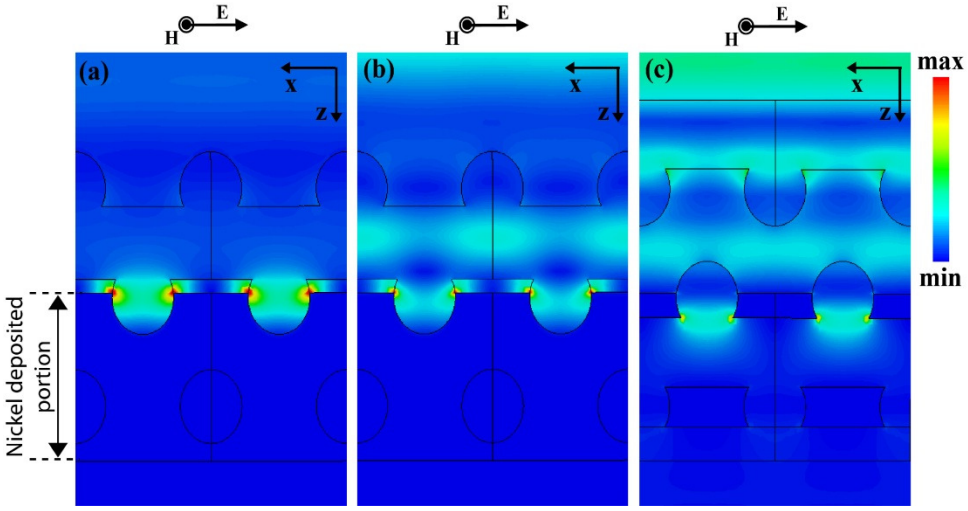

Fig. 4. (a) Amplitude plot of the electric field distributions of the first reflection dip within the nickel inversed woodpile MPC at λ = 2.4 µm (b) Amplitude plot of the electric field distributions of the second reflection dip at λ = 2.1 µm. (c) Amplitude plot of the electric field distributions of the third reflection dip at λ = 1.84 µm. The scale bar applies to all the figures.

To investigate further the absorption peaks within the inversed woodpile nickel MPC structure we inspect the electric field distributions for the first three reflection dips starting from the one at the longest wavelength. The reflection dips occur in different frequencies and the spatial distribution of the electric fields within the MPC depend on the corresponding wavelengths. We take the electric field distribution plots in the spectral positions of the reflection dips within the *x*-*z* cross-sections for different positions of *y* for which the field enhancement is maximum. Figure 4(a) shows the amplitude plot of the electric field distributions of the first reflection dip at the wavelength of 2.40 µm for a 25° angle of incidence. It can be seen that the electric fields couple very strongly to the opening of the dielectric cavity formed in the top portion of the deposited nickel film. The fields are strictly bound to the metallic surfaces within the cavity. The polarization direction of the incident fields and the orientation of the highly enhanced and confined fields within the cavity clearly suggest that the sharp reflection dip formed at the wavelength of 2.4 µm is due to the excitation of the localized plasmon resonances. We then look at the electric fields plot of the second reflection dip at the wavelength of 2.1 µm. The amplitude plot of the electric fields in Fig. 4(b) depicts almost a similar type of electric field distributions as in Fig. 4(a) where a strong localized field enhancement can be observed. This again suggests an enhanced light-

#169293 - $15.00 USD Received 24 May 2012; revised 28 Jun 2012; accepted 28 Jun 2012; published 2 Jul 2012

matter interaction with the excitation of localized plasmon resonances and hence, enhanced absorption.

Figure 4(c) shows the electric field distributions of the third reflection dip at the wavelength of 1.84 μm in the *x*-*z* cut plane. Interestingly, a weak field enhancement was observed at the metal-dielectric interface within the cavity formed in the top portion of the nickel film as depicted in Fig. 4(c). However, the fields are not totally confined within the cavity rather decouple from the cavity at the end, which indicates the nature of a propagating mode. Indeed, Fig. 3(b) shows that there exists a transmission band (although weak in magnitude, the finite transmission indicates a pass band, i.e. propagating modes) which starts at the vicinity of the third reflection dip at the wavelength of 1.84 μm. This suggests that the reflection dip (enhanced absorption) for the propagating mode at the wavelength of 1.84 μm is caused by the enhanced light-matter interaction at the photonic band edge [9–11]. For further clarification we have also thoroughly checked that this propagating nature of the mode does not exist for the first and second reflections dips at the wavelengths of 2.4 μm and 2.1 μm. This certainly confirms that the enhanced absorption at the wavelength of 1.84 μm is due to the periodicity induced enhanced light-matter interaction at the vicinity of the photonic band edge within the MPC environment. Thus the inversed woodpile nickel MPC structure contains unique features of resonant absorptions driven by localized plasmon resonances and also enhanced interactions within the photonic band edge.

4. Conclusions

In summary, we have demonstrated enhanced absorptions in the optical wavelengths within 3D inversed woodpile MPCs. Our low cost fabrication method presents the novelty of combining the state-of-the-art DLW method for dielectric PC template fabrication and the electrodeposition method for metal deposition for the realization of the 3D inversed woodpile nickel MPC structures. The fabricated MPCs show the unique optical properties of enhanced optical absorptions over a broad spectral range, which is consistent with the detailed numerical simulations. The experimental and theoretical investigations reveal two distinct mechanisms for the observed absorption enhancement, the resonant optical absorption caused by localized plasmon resonances and the photonic band edge induced enhanced optical absorption. Our MPC designs could thus be useful for applications in plasmonic solar cells [15–17] and for efficient tailored thermal radiation emission [8,12,14].

Acknowledgments

This research was conducted by the Australian Research Council Centre of Excellence for Ultrahigh bandwidth Devices for Optical Systems (project number CE110001018). Md M Hossain acknowledges the useful discussions on the experimental works with Baohua Jia, Dario Buso, and Joel Van Embden.